An Electromagnetic Ping-Pong Algorithm for Planar Reflector Antennas of Arbitrary Shapes

Shaolin Liao, *Senior Member, IEEE,* and Lu Ou, *Member, IEEE*

***Abstract*—An efficient Ping-Pong algorithm is presented to deal with electromagnetic scattering from planar reflector antennas of arbitrary geometric shapes. The proposed Computational Electromagnetics (CEM) algorithm does not require formation, storage and inverse of the impedance matrix used by the Method of Moments (MoM). Instead, a rigorous formula is obtained for computation of the surface current from the scattering electric field. Besides, the algorithm only contains convolution operations with the scalar Green's function and second derivatives operations to iteratively update the surface currents and scattering electric field. Also, hypersingular integration arising from the singularities of the surface current and scattering electric field is properly regularized. Furthermore, the algorithm converges fast and satisfactory results are obtained after a few iterations. Besides, the first iteration gives the solution for reflector antennas on perfect absorption substrates. Numerical solutions are obtained for some typical antennas and comparisons are made to those in the literature and from the MoM.**

***Index Terms*—Electromagnetic scattering, reflector antennas, convolution, singularity, hypersingular integration, scalar Green's function, Method of Moments (MoM), Computational ElectroMagnetics (CEM).**

I. Introduction

PLANAR reflector antennas and arrays have many important applications such as smart phased array electromagnetic wave steering [1] and programmable metasurfaces for radiation pattern control [2]. Careful designs of the reflector antennas and arrays are required to achieve the specific performance such as low Radar Cross Section (RCS [3]) and better antenna radiation patterns [4].

However, the accurate simulation of the electromagnetic scattering of the planar reflector antennas and arrays is challenging, partly due to the boundary edge effect of the reflector antennas, which usually generates singularities in surface current and scattering electromagnetic field [5], [6]. So efficient Computational ElectroMagnetics (CEM) methods are much needed. For electromagnetic scattering from metallic objects, the Method of Moments (MoM [7]) has been extensively used for computation of electromagnetic scattering of metallic objects. The MoM solves the Maxwell's equations based on the the Electric Field Integral Equation (EFIE [8]), one of the Surface Integral Equations (SIEs [9], [10]). For objects other than metals such as dielectric objects, the Magnetic Field Integral Equation (MFIE) and the combination of the EFIE and the MFIE, *i.e.*, the Combined Field Integral Equation (CFIE) [11]. The MoM surface current solution of the EFIE can be obtained through inverse of the MoM impedance matrix that is constructed as follows: 1) surface meshing — dividing the metallic object surface into many electrically small unit cells; 2) surface current basis representation — then the surface current within each unit cell is expressed in terms of the sum of some basis functions like Rao-Wilton-Glisson (RWG) basis [12], [13]; 3) electromagnetic field computation — electric field on all surface unit cells due to the surface current is computed; 4) test of the MoM boundary condition — test basis functions are used to obtain the MoM matrix equation that consists of the left-side product of the surface current vector under its basis function and the impedance matrix constructed through the inner product the scattering electric field and the test basis on the left and the surface current basis function on the right; as well as the right-side incident electromagnetic electric field vector under the test basis; and 5) solving of the unknown surface current vector — perform inverse of the MoM impedance matrix to obtain the unknown surface current vector under its basis function through some numerical matrix solver such as the conjugate gradient method.

The MoM CEM method has its own advantages compared with other methods such as the Finite Elements Method (FEM) and the Finite Difference Time Domain (FDTD) method. Firstly, the MoM only requires calculation of the electromagnetic field and storage of the surface current on the boundary surface, greatly reducing the computational effort and storage resource. Secondly, fast electromagnetic field propagation methods such as the Fast Multipole Method (FMM [14]) and the Fast Fourier Transform (FFT [10], [15]) method are readily available to accelerate the MoM impedance matrix computation. At last but not the least, efficient matrix inverse algorithms [16], [17], [18] such as the iterative Generalized Minimal REsidual Method (GMRES [18]) can be used to solve the MoM equation.

Even though the above advantages of the MoM, it has its own issues: first, the surface has to be discretized into complex mesh unit cells such as RWG triangles. then the careful choice of the basis function is required for accurate representation of the problem. also, the large impedance matrix has to be stored during the computation, whose size grows as N^2, with N being the number of unit cells. What's more important, inverse of the impedance matrix is required — even with efficient iterative algorithm such as GMRES, careful pre-conditioning and many iterations are required to obtain accurate solution. Finally, MoM doesn't work so well when the surface current contains singularities, which is the case of the electromagnetic scattering from the reflector antennas. This is because, around the singularities of the surface current, much

Shaolin Liao (Corresponding Author: liaoshlin@mail.sysu.edu.cn) is with School of Electronics and Information Technology, Sun Yat-sen University, Guangzhou, Guangdong Province, China.

Lu Ou is with College of Computer Science and Electronic Engineering, Hunan University, Changsha, Hunan, China 410082. She was partly supported by China Postdoctoral Science Foundation No. 2020M672488.

denser mesh is required. This means that the number of unit cell N becomes too large, and the size of the impedance matrix N^2 grows so fast that the inverse of the impedance matrix becomes increasingly intractable. From these aspects, it would be really helpful if no impedance matrix forming and inverse are involved to obtain the solution of the surface current, which is the focus of this paper: to develop some electromagnetic algorithm without impedance matrix. The main contribution of this paper is summarized as follows,

1) A Ping-Pong algorithm without impedance matrix forming, storage and inverse: both the surface current and the scattering electromagnetic field are updated alternatively and iteratively.
2) Rigorous formulas of the forward propagation operator and its inverse operator: the forward propagation operator is to obtain the scattering electromagnetic field from the surface current and the inverse operator is to obtain the surface current from the scattering electromagnetic field.
3) Simple computation: only convolution with the scalar Green's function and the following second derivatives are required to iteratively update the surface current and scattering electromagnetic field.
4) Hypersingular integration regularization: the hypersingular integration arising from the singularities of the surface current and the scattering electric field around the antenna boundary edges is properly regularized.
5) Fast convergence: the first iteration of the Ping-Pong algorithm gives the solutions of reflector antennas on perfect absorption substrates and it usually takes a few iterations to converge to satisfactory results.

The organization of this paper is as follows. Section II formulate the problem studied. Followed by Section III, where the electromagnetic field is represented in the 2D Fourier spectral domain. Then, Section IV presents the Ping-Pong algorithm. After that, numerical validation is shown in Section V, followed by discussion in Section VI. Finally, Section VII concludes the paper.

II. Problem Formulation

The electromagnetic scattering problem is shown in Fig. 1. The electromagnetic source field is incident upon some planar metallic reflector antenna (the square, disc, star and triangle here) and the goal is to solve for the unknown surface current. Imposing zero total electric field boundary condition on the metallic surface, the EFIE is obtained, as given Eq (1),

$$\left[\overline{E}^s_{//}(x,y) + \overline{E}^i_{//}(x,y)\right] \Omega(x,y) = 0, \tag{1}$$

where Ω is the binary mask that defines the geometry area of the reflector antenna; the superscripts s and i denote the scattering and incident electric field, respectively. Also, $\overline{E}^s_{//}(x,y)$ and $\overline{E}^i_{//}(x,y)$ are the scattering electric field and incident electric field on $x-y$ plane without the $\hat{z}$ component, respectively,

$$\overline{E}^{s,i}_{//}(x,y) = \hat{x}E^{s,i}_x(x,y) + \hat{y}E^{s,i}_y(x,y).$$

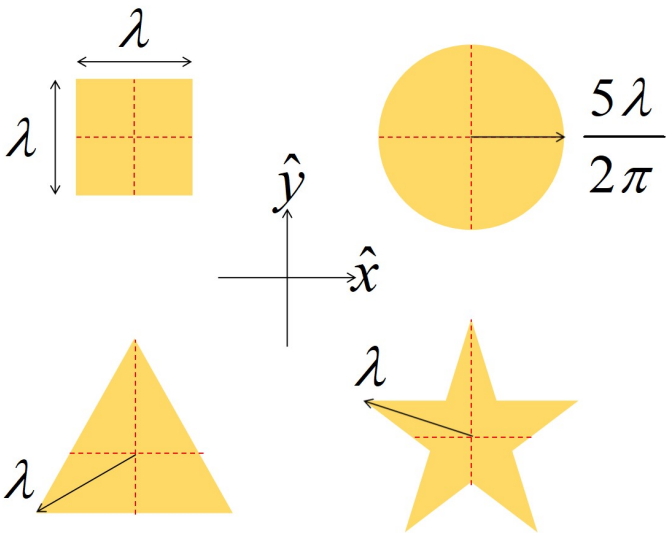

Figure 1. Electromagnetic scattering of planar reflector antennas of arbitrary shapes (clockwise): a square antenna of length $L_x = L_y = 1\lambda$, a circular disc antenna of radius $R = 5\lambda/(2\pi)$ or $kR = 5$, a star antenna of radius $R = \lambda$, and an equilateral triangle antenna of radius $R = 1\lambda$. Dashed lines denote where the surface currents are evaluated in the numerical simulation.

The scattering electric field $\overline{E}^s$ can be expressed in terms of convolution of the surface current $\mathbf{J}$ and the electric dyadic Green's function $\overline{\overline{G}}_e$, as shown in Eq (2),

$$\begin{aligned}\frac{\overline{E}^s(x,y)}{-j\omega\mu} &= \overline{\overline{G}}_e(x,y) \circledast \overline{J}(x,y) \\ &= \int_{-\infty}^{\infty}\int_{-\infty}^{\infty} \overline{\overline{G}}_e(x-x',y-y')\overline{J}(x',y')dx'dy',\end{aligned} \tag{2}$$

where $\circledast$ denotes the 2D convolution operation; ω is the angular frequency; μ is the permeability; and the electric dyadic Green's function is given as Eq (3),

$$\overline{\overline{G}}_e(\overline{r}) = g(\overline{r})\overline{\overline{I}} + \frac{1}{k^2}\nabla\nabla g(\overline{r}), \tag{3}$$

where $\overline{\overline{I}}$ is the identity matrix; k is the magnitude of the wave vector $\overline{k} = [k_x, k_y, k_z]$; and $g(\mathbf{r})$ is the scalar Green's function at the observation point vector $\overline{r} = [x, y, z]$,

$$g(r) = \frac{e^{-jkr}}{4\pi r}, \quad r = |\overline{r}|\,; \quad k = |\overline{k}| = \omega\sqrt{\mu\epsilon}.$$

III. Electromagnetic Field in the 2D Fourier Spectral Domain

Due to the planar geometry of the reflector antennas, it is convenient to express the electromagnetic field in terms of plane wave superposition in the Fourier spectral domain [19], [20].

A. Spectrum of the Scalar Green's Function

According to Weyl's identity [21], [22], [23], the scalar Green's function can be expressed in terms of plane wave

superposition as follows,

$$g(\overline{r}-\overline{r}') = \frac{e^{-jk|\overline{r}-\overline{r}'|}}{4\pi\,|\overline{r}-\overline{r}'|} = \int_{-\infty}^{\infty}\int_{-\infty}^{\infty} \frac{e^{j\overline{k}\cdot\overline{r}'}}{j4\pi k_z} e^{-j\overline{k}\cdot\overline{r}} dk_x dk_y, \quad (4)$$

which is valid when the observation point $\mathbf{r}$ is above the source point $\mathbf{r}'$, *i.e.*, $z > z'$; also k_z is the wavevector along z direction given by,

$$k_z = \begin{cases} \sqrt{k^2 - k_x^2 - k_y^2} & \text{for} \quad \sqrt{k_x^2+k_y^2} \le k, \\ -j\sqrt{k_x^2+k_y^2-k^2} & \text{for} \quad \sqrt{k_x^2+k_y^2} > k. \end{cases}$$

From Eq. (4), the 2D Fourier transform pair is then obtained as follows,

$$g(x,y) \Longleftrightarrow \mathcal{G}(k_x,k_y) = \frac{-j}{4\pi k_z} e^{-j\left(k_x x' + k_y y' + k_z z'\right)}, \quad (5)$$

where

$$\mathcal{G}(k_x,k_y) = \frac{1}{2\pi}\int_{-\infty}^{\infty}\int_{-\infty}^{\infty} g(x,y) e^{j(k_x x + k_y y)}\, dx\, dy,$$
$$g(x,y) = \frac{1}{2\pi}\int_{-\infty}^{\infty}\int_{-\infty}^{\infty} \mathcal{G}(k_x,k_y) e^{-j(k_x x + k_y y)}\, dk_x\, dk_y.$$

Similarly, when the observation point $\mathbf{r}$ is beneath the source point $\mathbf{r}'$, *i.e.*, $z < z'$, the 2D Fourier spectrum of the scalar Green's function is given by

$$g(x,y) \Longleftrightarrow \mathcal{G}(k_x,k_y) = \frac{-j}{4\pi k_z} e^{-j\left(k_x x' + k_y y' - k_z z'\right)}, \quad (6)$$

In particular, when the source point is set to the origin $\mathbf{r}' = 0$, the following is obtained,

$$g(x,y) \Longleftrightarrow \mathcal{G}(k_x,k_y) = \frac{-j}{4\pi k_z}. \quad (7)$$

B. Spectra of Derivatives of the Scalar Green's Function

With the 2D Fourier spectrum of the scalar Green's function given in Eq. (5), the spectra of the derivatives of the scalar Green's function are readily obtained.

Lemma 1. *The 2D Fourier transform pairs of the derivatives of the scalar Green's function are*

$$\frac{\partial^n}{\partial x^n} g_x(x,y) \Longleftrightarrow \mathcal{G}_x^{(n)}(k_x,k_y) = \frac{(-j)^{n+1}}{4\pi}\frac{k_x^n}{k_z},$$
$$\frac{\partial^n}{\partial y^n} g_y(x,y) \Longleftrightarrow \mathcal{G}_y^{(n)}(k_x,k_y) = \frac{(-j)^{n+1}}{4\pi}\frac{k_y^n}{k_z},$$
$$\frac{\partial^n\partial^{n'}}{\partial x^n \partial y^{n'}} g(x,y) \Longleftrightarrow \mathcal{G}_{x,y}^{(n,n')}(k_x,k_y) = \frac{(-j)^{n+n'+1}}{4\pi}\frac{k_x^n k_y^{n'}}{k_z},$$

where the superscript n denotes the order of derivative and the subscript x, y denotes the variable the derivative takes on.

Proof: Taking the derivatives on the observation point $\mathbf{r}$ of Eq. (4), **Lemma 1** can be proved. ■

C. Spectrum of the Electric Dyadic Green's Function

The 2D Fourier spectrum of the electric dyadic Green's function can be obtained from its definition in Eq. (3) and **Lemma 1**.

Lemma 2. *The 2D Fourier transform pair of the electric dyadic Green's function is*

$$\overline{\overline{G}}_e(\mathbf{x},\mathbf{y}) \Longleftrightarrow \overline{\overline{\mathcal{G}}}_e(k_x,k_y) = -\frac{2\pi\delta(z)}{k^2}\hat{z}\hat{z} - \frac{j}{4\pi k_z}\left(\overline{\overline{I}} - \hat{k}\hat{k}\right),$$

where $\hat{k}$ is the unit wave vector $\hat{k} = \overline{k}/k$; and $\hat{k}\hat{k}$ can be considered as a matrix working on an input current spectrum vector on its right side (the dot product of the right $\mathbf{k}$*) and producing an output electric field spectrum vector (the left* $\mathbf{k}$*).*

Proof: The first term of the electric dyadic Green's function $\overline{\overline{G}}_e$ in Eq. (3) is the product of the scalar Green's function with a constant identity matrix, whose 2D Fourier spectrum is just $\mathcal{G}(k_x,k_y)\overline{\overline{I}}$. The second term of the electric dyadic Green's function $\overline{\overline{G}}_e$ can be expanded into the sum of all second derivatives whose 2D Fourier spectra can be obtained from **Lemma 1**. At last, the $\hat{z}\hat{z}$ term is due to the change of electromagnetic wave propagation direction from $+\hat{z}$ to the $-\hat{z}$, as shown in Eq. (5) and Eq. (6), respectively. ■

D. Spectrum of the Scattering Electric Field

The 2D Fourier spectrum of the scattering electric field $\mathbf{E}^s$ in Eq. (2) is the product of the spectrum of the surface current $\overline{\mathcal{J}}$ and the spectrum of the electric dyadic Green's function.

Lemma 3. *The 2D Fourier spectrum of the scattering field is given by*

$$\overline{\mathcal{E}}^s(k_x,k_y) = -\frac{\omega\mu}{2k_z}\left(\overline{\overline{I}} - \hat{k}\hat{k}\right)\overline{\mathcal{J}}\,(k_x,k_y)\,. \quad (8)$$

Proof: According to the convolution property of the Fourier transform, the spectrum of the scattering field is the product of the spectrum of the surface current and the spectrum of the dyadic Green's function given in **Lemma 2**. ■

IV. The Ping-Pong Algorithm of the Electromagnetic Scattering Problem

In the proposed Ping-Pong algorithm, the solution of the scattering electromagnetic field can be obtained first in the 2D Fourier spectral domain and then transformed back to the spatial domain.

A. Scattering Electric Field Radiated by Surface Currents

The scattering electric field can be expressed as the convolution of the surface current with the dyadic Green's function in Eq. (2). It contains higher-order singularities due to the derivatives on the scalar Green's function [26], which can be reduced to only convolutions with the scalar Green's function.

Lemma 4. *The scattering electric field can be expressed in terms of only convolution with the scalar Green's function kernel and second derivatives after that,*

$$\begin{aligned}\overline{E}^s(x,y) &= \mathscr{L}\left\{\overline{J}(x,y)\right\} \qquad (9)\\ &= \frac{\omega\mu}{j}\left\{\overline{\overline{I}} + \frac{1}{k^2}\begin{bmatrix}\frac{\partial^2}{\partial x^2} & \frac{\partial^2}{\partial x\partial y} & \frac{\partial^2}{\partial x\partial z}\\ \frac{\partial^2}{\partial x\partial y} & \frac{\partial^2}{\partial y^2} & \frac{\partial^2}{\partial y\partial z}\\ \frac{\partial^2}{\partial x\partial z} & \frac{\partial^2}{\partial y\partial z} & \frac{\partial^2}{\partial z^2}\end{bmatrix}\right\}\left[g(x,y)\circledast\overline{J}(x,y)\right],\end{aligned}$$

where $\mathscr{L}$ is the forward propagation operator.

Proof: The differential operators are on the source point coordinate $\overline{r}'$ of the scalar Green's function in Eq. (2), which can be first transferred to the observation point coordinate $\overline{r}$,

$$\begin{aligned}\frac{\overline{E}^s(x,y)}{-j\omega\mu} =& \overline{\overline{I}}g(x,y)\circledast\overline{J}(x,y)+ \qquad (10)\\ &\frac{1}{k^2}\int_{-\infty}^{\infty}\int_{-\infty}^{\infty}\nabla\nabla g(x-x',y-y')\overline{J}(x',y')dx'dy'.\end{aligned}$$

where the following relations have been used,

$$\begin{aligned}\nabla' g(x-x',y-y') &= -\nabla g(x-x',y-y'),\\ \nabla'\nabla' g(x-x',y-y') &= \nabla\nabla g(x-x',y-y').\end{aligned}$$

with ∇' denoting the derivative on the source point $\overline{r}'$.

Then the derivatives on the observation point coordinate $\overline{r}$ in Eq. (10) can be further transferred outside the integral and **Lemma 4** is proved. ∎

In particular, for the problem of 2D electromagnetic scattering from planar reflector antennas, Eq. (9) in **Lemma 4** reduces to the following,

$$\begin{aligned}\overline{E}^s(x,y) &= \mathscr{L}\left\{\overline{J}(x,y)\right\} \qquad (11)\\ &= \frac{\omega\mu}{j}\left\{\overline{\overline{I}} + \frac{1}{k^2}\begin{bmatrix}\frac{\partial^2}{\partial x^2} & \frac{\partial^2}{\partial x\partial y}\\ \frac{\partial^2}{\partial x\partial y} & \frac{\partial^2}{\partial y^2}\\ \frac{\partial^2}{\partial z\partial x} & \frac{\partial^2}{\partial z\partial y}\end{bmatrix}\right\}\left[g(x,y)\circledast\overline{J}(x,y)\right].\end{aligned}$$

B. Surface Current from the Scattering Electric Field

The the surface current can be obtained from the scattering electric field $\mathbf{E}^s$, which is the inverse process of **Lemma 4**.

Lemma 5. *The surface current can be expressed in terms of the scattering electric field as*

$$\begin{aligned}\overline{J}(x,y) &= \mathscr{L}^{-1}\left\{\overline{E}^s(x,y)\right\} \qquad (12)\\ &= \frac{4\omega\epsilon}{j}\left\{\overline{\overline{I}} + \frac{1}{k^2}\begin{bmatrix}\frac{\partial^2}{\partial y^2} & -\frac{\partial^2}{\partial x\partial y}\\ -\frac{\partial^2}{\partial xy} & \frac{\partial^2}{\partial x^2}\end{bmatrix}\right\}\left[g(x,y)\circledast\overline{E}^s_{//}(x,y)\right],\end{aligned}$$

where $\mathscr{L}^{-1}$ is the inverse operator of the forward propagation operator $\mathscr{L}$ given in Eq. (9) of **Lemma 4***; ϵ is the permittivity.*

Proof: With the help of **Lemma 3**, the 2D Fourier spectrum of the surface current $\overline{\mathcal{J}}(k_x,k_y)$ can be solved in the spectral domain of the EFIE equation in Eq. (1),

$$\begin{aligned}\mathcal{J}_x(k_x,k_y) &= \frac{-2}{\omega\mu}\left[\frac{k^2-k_y^2}{k_z}\mathcal{E}^s_x(k_x,k_y)+\frac{k_xk_y}{k_z}\mathcal{E}^s_y(k_x,k_y)\right],\\ \mathcal{J}_y(k_x,k_y) &= \frac{-2}{\omega\mu}\left[\frac{k^2-k_x^2}{k_z}\mathcal{E}^s_y(k_x,k_y)+\frac{k_xk_y}{k_z}\mathcal{E}^s_x(k_x,k_y)\right],\end{aligned}$$

from which it can be seen that the 2D Fourier spectrum of the surface current can be re-written in terms of the product of the 2D Fourier spectrum of the scalar Green's function and the 2D Fourier spectrum of the incident electric field, as well as the $k_x^mk_y^n, m=1,2$ terms,

$$\begin{aligned}\mathcal{J}_x(k_x,k_y) =& \frac{-j8\pi}{\omega\mu}\left[\left(k^2-k_y^2\right)\mathcal{G}(k_x,k_y)\mathcal{E}^s_x(k_x,k_y)+\right.\\ &\left.k_xk_y\mathcal{G}(k_x,k_y)\mathcal{E}^s_y(k_x,k_y)\right],\\ \mathcal{J}_y(k_x,k_y) =& \frac{-j8\pi}{\omega\mu}\left[\left(k^2-k_x^2\right)\mathcal{G}(k_x,k_y)\mathcal{E}^s_y(k_x,k_y)+\right.\\ &\left.k_xk_y\mathcal{G}(k_x,k_y)\mathcal{E}^s_x(k_x,k_y)\right].\end{aligned}$$

Then the 2D inverse Fourier transform in the spatial domain gives the convolution of the scalar Green's function with the incident electric field,

$$2\pi\mathcal{G}(k_x,k_y)\mathcal{E}^s_u(k_x,k_y)\Longleftrightarrow g(x,y)\circledast E^s_u(x,y),\quad u=x,y.$$

Finally the $k_x^mk_y^n, m=1,2$ terms correspond to the derivatives of the convolution in the spatial domain and **Lemma 5** is proved. ∎

Eq. (12) in **Lemma 5** is believed to appear for the first time and is the main result of this paper that leads to the following Ping-Pong algorithm.

C. The Ping-Pong Algorithm

With the help from **Lemma 4** and **Lemma 5**, the solutions of the surface current and scattering electric field can be obtained according to the EFIE, as shown in Eq. (1).

Theorem 6. *The surface current and scattering electric field can be updated iteratively as follows,*

$$\overline{J}_{n+1}(x,y) = \mathscr{L}^{-1}\left\{\overline{\Omega}\ \overline{E}^s_{//,n}(x,y) - \Omega\ \overline{E}^i_{//}(x,y)\right\}, \qquad (13)$$

$$\overline{E}^s_{n+1}(x,y) = \mathscr{L}\left\{\Omega\overline{J}_{n+1}(x,y)\right\}, \qquad (14)$$

where $\overline{\Omega}=1-\Omega$ is the complementary area of the reflector antenna.

Proof: There are two constraints according to the EFIE equation in Eq. (1): 1) the scattering electric field cancel the incident electric field on the surface of the reflector antenna, *i.e.*, $\overline{E}^s_{//}(x,y) = -\overline{E}^i_{//}(x,y)$; and 2) the surface current only exists on the surface of the reflector antenna, *i.e.*, $\overline{\Omega}\ \overline{J}(x,y) = 0$. Eq. (13) is obtained from constraint 1) according to Eq. (12) of **Lemma 5** and Eq. (14) is obtained from constraint 2) according to Eq. (9) of **Lemma 4**. ∎

In particular, the first iteration of **Theorem 6** gives solution for the perfect absorption substrate: the scattering electric field

only exists on the reflector antenna surface and disappear outside the reflector antenna surface,

$$\overline{E}^s_{//}(x,y) = -\Omega\overline{E}^i_{//}(x,y), \quad \overline{\Omega}\ \overline{E}^s_{//}(x,y) = 0,$$

with the solution of the surface current given by,

$$\overline{J}_1(x,y) = -\mathscr{L}^{-1}\left\{\Omega\overline{E}^i_{//}(x,y)\right\}. \tag{15}$$

D. Singularities Regularization

Besides the regular singularity of the scalar Green's function, the surface current and scattering electric field could contains singularities around the antenna boundary edges due to the the derivatives operations after the convolution with the scalar Green's function, as shown in the forward propagation operator in **Lemma 4** and the inverse operator in **Lemma 5**. These singularities have to be regularized before integration [24], [25], [26], [27].

Two types of singular integration are met during the iteration of the Ping-Pong algorithm:

1) Regular singular integration: for observation point $\overline{r}$ that is not at the singularities of the surface current or the scattering electric field around the antenna boundary edges $\partial\Omega$, the integration can be readily regularized [27]. Because there are two types of regular singularities, one from the scalar Green's function and the other from the surface current or scattering electric field, the integration domain can be divided into two sub-domains around these two singularities, besides the rest of the sub-domain.

   For example, consider the point-type singularities of the surface current around the antenna corners in the convolution integration of the surface current with the scalar Green's function of **Lemma 4**: First, in the sub-domain around the singularity of the scalar Green's function, denoted as Ω_g,

$$\begin{aligned} I^{\Omega_g}_{\circledast} &= g(x,y) \circledast \overline{J}(x,y)\big|_{\Omega_g} \\ &= \iint\limits_{\Omega_g} \frac{e^{-jkr'}}{4\pi}\overline{J}(r',\phi')dr'd\phi', \end{aligned}$$

   where the observation point has been set to the origin $(0,0)$. Then, in the sub-domain around the singularity of the surface current, denoted as Ω_J,

$$I^{\Omega_J}_{\circledast} = \iint\limits_{\Omega_J} \frac{e^{-jkr'}}{4\pi|\overline{r}' - \overline{r}_o|}\left[r'\overline{J}(r',\phi')\right]dr'd\phi',$$

   where $I^{\Omega_J}_{\circledast}$ is defined similarly as $I^{\Omega_g}_{\circledast}$; also the origin of the polar coordinate has been set to the singularity point of the surface current and $\overline{r}_o$ is the observation point in this local coordinate. Now the regularized surface current $r'\overline{J}(r',\phi')$ should contain no singularities and the integration can be readily evaluated.

   Similarly, the line-type singularities of the surface current around the edges of the antenna boundary edges can be done similarly [27] in the local Cartesian coordinate. Finally, the integration in the sub-domain other than Ω_g and Ω_J can be done through quadrature methods.

2) Hypersingular integration: for observation point $\overline{r}$ that is at the singularities of the surface current or the scattering electric field around the antenna boundary edges $\partial\Omega$, both the regular singularity of the scalar Green's function and the singularities of the surface current or the scattering electric field exist. This is the hypersingular integration [28] that can be done in the following steps: 1) similar to the regular singular integration above, first remove the regular singularity of the scalar Green's function in the polar coordinate; 2) then, divide the integration domain into two sub-domains: a small disc sub-domain around the singularity with radius δr, dentoed as Ω_δ, and the rest sub-domain; 3) after that, the radius of the small disc sub-domain Ω_δ is chosen such that the rest of the sub-domain can be accurately evaluated with the conventional quadrature integration method; 4) finally, the hypersingular integration [28] on the small disc sub-domain Ω_δ is performed. It is noted that only the singularity with $1/(r')^p, p \geq 1$ generates hypersingular equation; also, it is required that $p < 2$ or otherwise the solution will diverge everywhere. So only the hypersingular integration with $1 \leq p < 2$ is relevant,

$$\begin{aligned} I^{\Omega_\delta}_{\circledast} &= \iint\limits_{\Omega_\delta} \frac{e^{-jkr'}}{4\pi}\overline{J}(r',\phi')dr'd\phi', \\ &= \iint\limits_{\Omega_\delta} \frac{e^{-jkr'}}{4\pi}\frac{\overline{J}'(r',\phi')}{(r')^p}dr'd\phi', \end{aligned}$$

   where $I^{\Omega_\delta}_{\circledast}$ is defined similarly as $I^{\Omega_g}_{\circledast}$ and $1 \leq p < 2$ is the order of singularity such that $\overline{J}'(r',\phi') = \overline{J}(r',\phi')(r')^p$ is not singular. Then, the integration can be evaluated through Taylor expansion [28] of $\overline{J}'(r',\phi')e^{-jkr'}$, which contains the following singular part,

$$\int\limits_{r'=\sigma\to 0}^{\delta r}\int\limits_{\phi'=0}^{2\pi} \frac{\overline{J}'(0,0)}{4\pi}\frac{1}{r'}dr'd\phi' = C\ln(\delta r) - C\ln(\sigma),$$

   for $p = 1$ with $C = \overline{J}'(0,0)/2$; and

$$\int\limits_{r'=\sigma\to 0}^{\delta r}\int\limits_{\phi'=0}^{2\pi} \frac{\overline{J}'(0,0)}{4\pi}\frac{1}{(r')^p}dr'd\phi' = \frac{C'}{(\delta r)^{p-1}} - \frac{C'}{\sigma^{p-1}},$$

   for $1 < p < 2$ with $C' = \overline{J}'(0,0)/[2(1-p)]$. The second term is the scattering electric field singularity when $\sigma \to 0$: $\ln(\sigma)$ for $p = 1$ and $1/\sigma^{p-1}$ for $p > 1$. Similarly, the hypersingular integration due to the line-type singularities of the surface current around the antenna edges can be evaluated in the local Cartesian coordinate.

At last, similar treatment can be done for the hypersingular convolution integration of the singular scattering electric field with the scalar Green's function in Eq. (12) of **Lemma 5**.

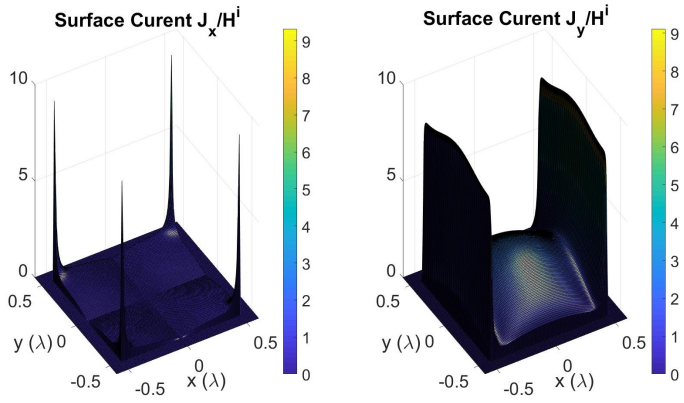

Figure 2. A square reflector antenna of length $L_x = L_y = 1$: surface currents J_x and J_y.

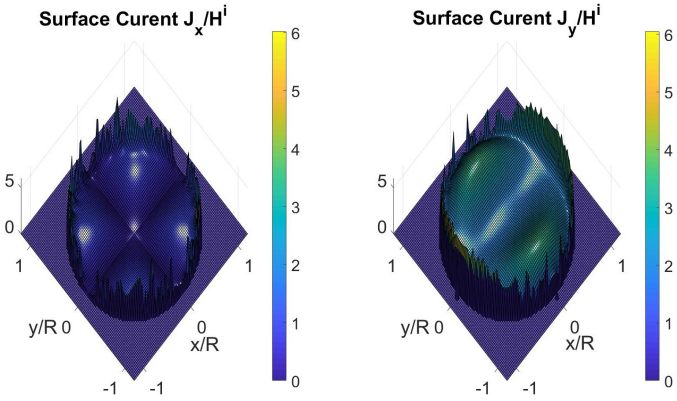

Figure 4. A disc reflector antenna of radius $R = 5\lambda/(2\pi)$ or $kR = 5$: surface currents J_x and J_y.

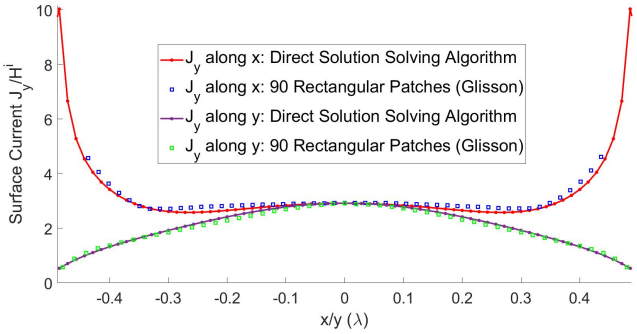

Figure 3. A square reflector antenna of length $L_x = L_y = 1$: line plots of surface current J_y J_x along $\hat{x}/\hat{y}$ directions and comparison with results from the literature [5].

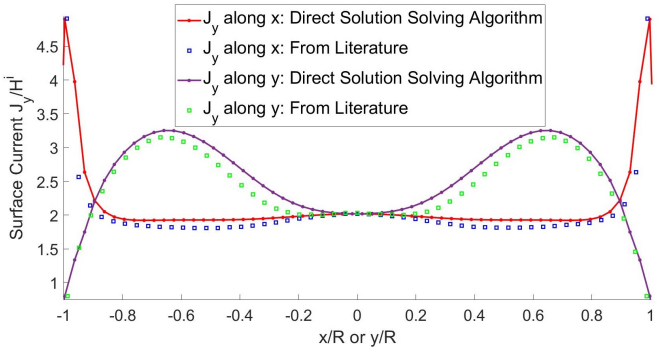

Figure 5. A disc reflector antenna of radius $R = 5\lambda/(2\pi)$ or $kR = 5$: line plots of surface current J_y along $\hat{x}/\hat{y}$ directions and comparison with results from the literature [6].

V. Numerical Simulations

Numerical solutions of four typical reflector antennas are obtained with the Ping-Pong algorithm: a square reflector antenna of length $L_x = L_y = 1\lambda$, a circular reflector disc antenna of radius $R = 5\lambda/(2\pi)$ or $kR = 5$, an equilateral triangle reflector antenna of radius $R = 1\lambda$ and a star reflector antenna of radius $R = 1\lambda$, as shown in Fig. 1. Comparisons of the solutions with those in the literature and from the MoM are also made. Also, without loss of generality, normal plane wave incidence with $\hat{y}$ polarization is used.

Firstly, Fig. 2 shows the surface currents J_x and J_y for the square reflector antenna of length $L_x = L_y = 1\lambda$, obtained with five iterations. It can see that the the surface current J_y (normalized to the incident magnetic field H^i) disappears on the antenna boundary edges that are perpendicular to $\hat{y}$ direction, which is due to the $\hat{y}$ polarization of the incidence electromagnetic wave. Also, the surface current J_y has line-type singularities around the antenna boundary edges that are perpendicular to $\hat{x}$ direction and the the surface current J_x has point-like singularities around the antenna corners. Then, Fig. 3 shows the comparison of results obtained from the Ping-Pong algorithm and those from the literature [5] using the MoM with a mesh of 90 rectangular patches: dominant surface current J_y is shown along both the $\hat{x}$ and $\hat{y}$ directions, as shown in Fig. 1, the red dotted line and blue squares are for the $\hat{x}$ direction and the purple dotted line and green squares are for the $\hat{y}$ direction. It can be seen that good agreement has been achieved.

Then, in Fig. 4, the surface currents J_x and J_y are shown for the circular disc antenna of radius $R = 5\lambda/(2\pi)$ or $kR = 5$, obtained with three iterations. It can be seen that singular surface current J_y happens on the antenna boundary edges that are perpendicular to the $\hat{x}$ direction, due to the $\hat{y}$-polarized incidence field. The surface current J_y shows the resonant characteristics distribution: two surface current peaks are on each side of the disc reflector antenna. Also, Fig. 5 shows the comparison of results obtained from the Ping-Pong algorithm and those from the literature [6]: dominant surface current J_y is shown along both the $\hat{x}$ and $\hat{y}$ directions. As shown in Fig. 1, the red dotted line and blue squares are for the $\hat{x}$ direction and the purple dotted line and green squares are for the $\hat{y}$ direction. It can be seen that all features of the surface current are obtained by the Ping-Pong algorithm.

Also, Fig. 6 shows surface current J_x and J_y for the triangle reflector antenna of radius $R = 1\lambda$, obtained with four iterations. Similarly, it can be seen that the surface current disappear on the antenna boundary edge that is perpendicular to the electric field polarization direction $\hat{y}$. Also, line-type singularities are observed along the edges that are not perpendicular to the electric field polarization direction $\hat{y}$ and point-type singularities are observed around the antenna vertices.

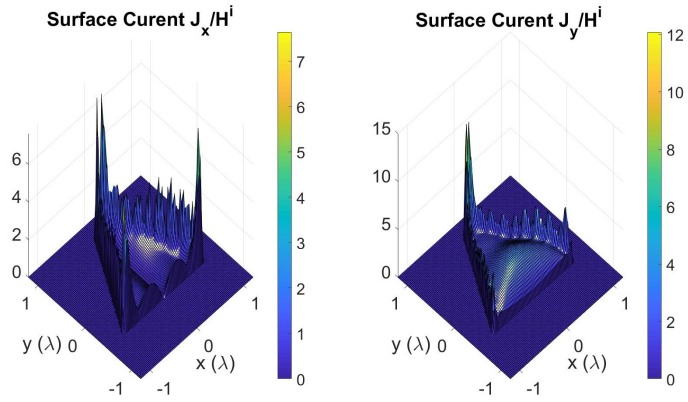

Figure 6. A triangle reflector antenna of radius $R = 1\lambda$: surface currents J_x and J_y.

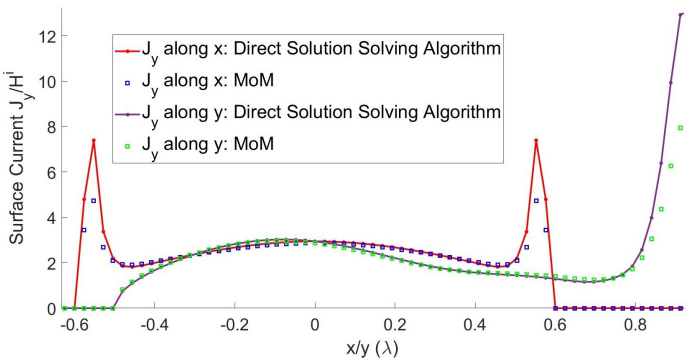

Figure 7. A triangle reflector antenna of radius $R = 1\lambda$: line plots of surface current J_y along $\hat{x}/\hat{y}$ directions and comparison with results of the MoM.

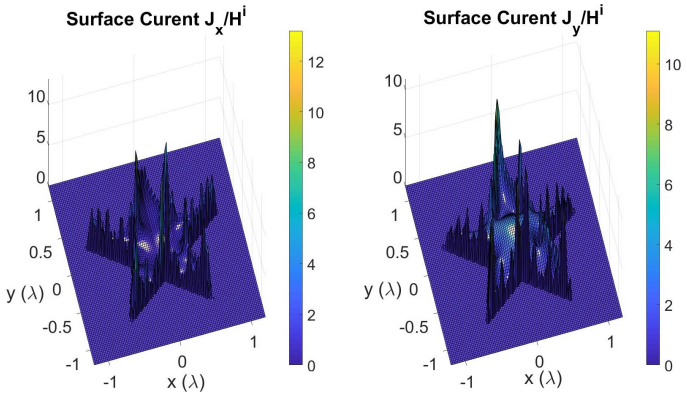

Figure 8. A star reflector antenna of radius $R = 1\lambda$: surface currents J_x and J_y.

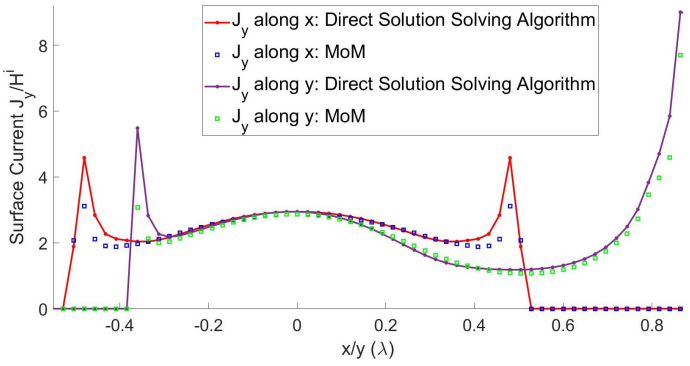

Figure 9. A star reflector antenna of radius $R = 1\lambda$: line plots of surface current J_y along $\hat{x}/\hat{y}$ directions and comparison with results of the MoM.

In particular, the surface current is the strongest at the top vortex of the triangle reflector antenna, which is the joining point of the surface current flows along both edges of the triangle reflector antenna. To show the validity of the Ping-Pong algorithm, the comparison with the results obtained from the MoM has been made in Fig. 7 for the dominant surface current J_y along both $\hat{x}$ and $\hat{y}$ directions (see Fig. 1): the red dotted line and blue squares are for $\hat{x}$ direction and the purple dotted line and green squares are for the $\hat{y}$ direction. It can be seen that the solution of the Ping-Pong algorithm can gives better result around the singularity point. This is mainly due to the finite size of the mesh used in the MoM, limiting its performance around the singularities.

Finally, Fig. 8 shows the surface currents J_x and J_y for the star reflector antenna of radius $R = 1\lambda$, obtained with 3 iterations. Again, it can be seen that line-type singularities happen around the antenna boundary edges and point-type singularities at the vertices of the star reflector antenna. Also, Fig. 9 shows the comparison of the results between the Ping-Pong algorithm and the MoM, which again shows good agreements in dominant surface current J_y in both $\hat{x}$ and $\hat{y}$ directions (see Fig. 1): the red dotted line and blue squares are for $\hat{x}$ direction and the purple dotted line and green squares are for the $\hat{y}$ direction.

At last, to show the convergence and the efficiency of the Ping-Pong algorithm, Fig. 10 compare the convergence performance of both algorithms, which clearly shows that the Ping-Pong algorithm outperforms the MoM: it converges in around 5 iterations, while the MoM converges in around 50 iterations, meaning 10 times as fast.

VI. Discussion

The proposed Ping-Pong algorithm is very efficient for the electromagnetic scattering of 2D metallic structures: it works in a straight-forward iteration way to sequentially update the surface current and the scattering electric field, with each other in the last update as input. Also, usually only a few iterations give satisfactory results. Besides, the first iteration of **Theorem 6** is the solution of the perfect absorption substrate, as shown in Eq. (15), which provides good initial solution of the Ping-Pong algorithm.

In addition, the numerical simulation confirms the singularities of the surface current around the antenna boundary edges that are not perpendicular to the polarization direction of the incidence electric field, as well as around the vertices of the antenna. These singularities generate hypersingular integration during the iteration of the Ping-Pong algorithm, whose treatment has been discussed in Section VI. More advanced hypersingular integration methods [29] would definitely improve the algorithm.

What's more, fast algorithms such as FFT [10], [15] and FMM [14] could be used to accelerate the computation of the

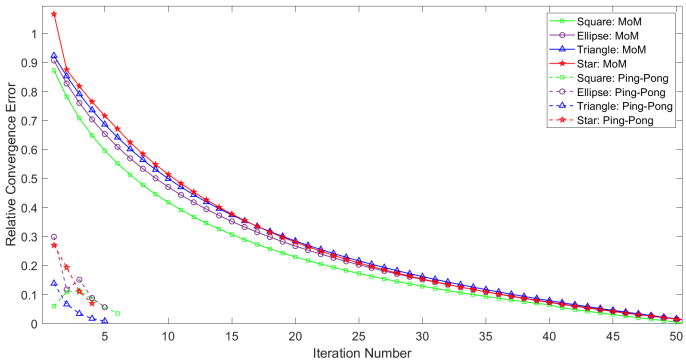

Figure 10. Convergence of the Ping-Pong algorithm and the MoM shows the efficiency of the Ping-Pong algorithm.

convolution with the scalar Green's function, further improving the efficiency of the Ping-Pong algorithm.

At last, although numerical simulations are only performed for individual reflector antennas in this paper, the Ping-Pong algorithm is expected to work equivalently well for 2D metallic antenna arrays and metasurfaces.

VII. Conclusion

The efficient Ping-Pong algorithm has been studied for the electromagnetic scattering problem of planar reflector antennas of arbitrary shapes. The algorithm does not compute, store and perform inverse of the impedance matrix required in the MoM. Instead, rigorous formulas have been obtained for the forward propagation operator for computation of the scattering electric field from the surface current and its inverse operator for computation of the surface current from the scattering electric field. Then, the algorithm interactively updates the surface current and scattering electric field with the forward propagation operator and its inverse, which consists of only convolutions with the scalar Green's function and the following simple second-order derivatives. Also, only regular singularities of the scalar Green's function is involved in the integral, greatly simplifying the integration. In addition, hypersingular integration that arises from the singularities of the surface current and the scattering field has been properly regularized. What's more, the Ping-Pong algorithm converges very fast and usually takes only a few iterations to obtain satisfactory results. In addition, the first iteration gives the solution of reflector antennas on perfect absorption substrates. Numerical simulation has been performed for four typical antennas, *i.e.*, a square, a disc, a triangle and a star. The comparisons to those of the literature and from the MoM show good agreements. At last, the algorithm is universal and very promising in simulation of other 2D metallic structures, including antenna arrays and metasurfaces.

References

[1] Y.-C. Liang, R. Long, Q. Zhang, J. Chen, H. V. Cheng, and H. Guo, "Large intelligent surface/antennas (LISA): Making reflective radios smart," *Journal of Communications and Information Networks,* vol. 4, no. 2, pp. 40-50, 2019.

[2] H. Yang, X. Cao, F. Yang, J. Gao, S. Xu, M. Li, X. Chen, Y. Zhao, Y. Zheng and S. Li, "A programmable metasurface with dynamic polarization, scattering and focusing control," *Scientific Reports,* vol. 6, no. 1, p. 35692, 2016.

[3] Z.-J. Han, W. Song, and X.-Q. Sheng, "In-band RCS reduction and gain enhancement for a patch antenna array by using a 1-D periodic metasurface reflector," *IEEE Transactions on Antennas and Propagation*, vol. 67, no. 6, pp. 4269-4274, 2019.

[4] S. K. Rao and C. Ostroot, "Design principles and guidelines for phased array and reflector antennas [Antenna Applications Corner]," *IEEE Antennas and Propagation Magazine*, vol. 62, no. 2, pp. 74-81, 2020.

[5] S. Rao, D. Wilton, and A. Glisson, "Electromagnetic scattering by surfaces of arbitrary shape," *IEEE Transactions on Antennas and Propagation,* vol. 30, no. 3, pp. 409-418, 1982.

[6] K. Hongo and Q. A. Naqvi, "Diffraction of electromagnetic wave by disk and circular hole in a perfectly conducting plane," *Progress In Electromagnetics Research*, Vol. 68, 113-150, 2007.

[7] E. Arvas and L. Sevgi, "A Tutorial on the Method of Moments [Testing Ourselves]," *IEEE Antennas and Propagation Magazine*, vol. 54, no. 3, pp. 260-275, 2012.

[8] R. F. Harrington, *Field Computation by Moment Methods*, New York: McMillan, 1968.

[9] W.C. Chew, J.M. Jin, E. Michielssen, J.M. Song, Eds., *Fast and Efficient Algorithms in Computational Electromagnetics*, Artech House, 2001.

[10] S. Liao, N. Gopalsami, A. Venugopal, A. Heifetz, and A. C. Raptis, "An efficient iterative algorithm for computation of scattering from dielectric objects," *Optics Express*, Vol. 19, No. 3, pp. 3304-3315, 2011.

[11] W. C. Chew, M. S. Tong, and B. Hu, *Integral Equations Methods for Electromagnetic and Elastic Waves*, Morgan & Claypool, 2008.

[12] S. M. Rao, D. R. Wilton, A. W. Glisson, "Electromagnetic Scattering by Surfaces of Arbitrary Shape", *IEEE Transactions on Antennas and Propagation*, vol. AP-30, no. 3, pp. 409-418, 1982.

[13] D. R. Wilton, S. M. Rao, A. W. Glisson, D. H. Schaubert, O. M. Al-Bundak, and C. M. Butler, "Potential integrals for uniform and linear source distributions on polygonal and polyhedral domains," *IEEE Transactions on Antennas and Propagation*, vol. AP-32, pp. 276-281, 1984.

[14] N. Engheta, W. D. Murphy, V. Rokhlin, and M. S. Vassiliou, "The Fast Multipole Method (FMM) for electromagnetic scattering problems," *IEEE Transactions on Antennas and Propagation,* vol. 40, no. 6, pp. 634-641, 1992.

[15] S. Liao and Vernon Ronald J., "A fast algorithm for computation of electromagnetic wave propagation in half-space," *IEEE Transactions on Antennas and Propagation*, Vol. 57, No. 7, pp. 2068-2075, 2009.

[16] S. M. Rao, A. W. Glisson, D. R. Wilton, and B. S. Vidula, "A simple numerical solution procedure for statics problems involving arbitrary shaped conductors," *IEEE Transactions on Antennas and Propagation*, vol. 27, pp. 604-607, 1979.

[17] R. Mittra, V. V. S. Prakash, and Soon Jae Kwon, "An improved iterative solution for method of moments problems in electromagnetics," *IEEE Antennas and Propagation Society International Symposium*, vol. 4, pp. 622-625, 2002.

[18] P. L. Rui, H. Yong, and R. S. Chen, "Multipreconditioned GMRES method for electromagnetic wave scattering problems," *Microwave and Optical Technology Letters*, vol. 50, no. 1, pp. 150–152, 2008.

[19] S. Liao, *Multi-frequency beam-shaping mirror system design for high-power gyrotrons: Theory, algorithms and methods*, Ph.D. Thesis, ProQuest Dissertations and Theses, Publication Number: AAI3314260, ISBN: 9780549633167, 2008.

[20] S. Costanzo and G. Di Massa, "Improved Spectral Iteration Technique for the Scattering by Thin Metal Plates," *Progress In Electromagnetics Research*, vol. 3, pp. 1-13, 2008.

[21] H. Weyl, "Ausbreitung elektromagnetischer Wellen über einem ebenen Leiter," *Ann. d. Phys.* 60, 481-500, 1919.

[22] J. A. Stratton, *Electromagnetic Theory*, p. 577., McGraw-Hill, New York, 1941.

[23] A. S. Marathay, "Fourier transform of the Green's function for the Helmholtz equation," *Journal of the Optical Society of America*, Vol. 65, No. 8, pp. 964-965, 1975.

[24] S.-W. Lee, J. Boersma, C.-L. Law, and G. Deschamps, "Singularity in Green's function and its numerical evaluation," *IEEE Trans. Antennas Propagat.*, vol. 28, no. 3, pp. 311-317, 1980.

[25] A. D. Yaghjian, "Electric dyadic Green's functions in the source region," *Proc. IEEE*, Vol. 68, 248-263, 1980.

[26] M. Tong and W. C. Chew, "A Novel Approach for Evaluating Hypersingular and Strongly Singular Surface Integrals in Electromagnetics,"

IEEE Transactions on Antennas and Propagation, vol. 58, no. 11, pp. 3593-3601, 2010.

[27] S. Amari and J. Bornemann, "Integrals with Applications to Electromagnetics," *IEEE Transactions on Antennas and Propagation*, Vol. 43, No. 11, pp. 1343-1348, 1995.

[28] G. Monegato, "Numerical evaluation of hypersingular integrals," *Journal of Computational and Applied Mathematics*, vol. 50, no. 1, pp. 9-31, 1994.

[29] C. Lee, H. Wang, and Q. Qin, "Efficient hypersingular line and surface integrals direct evaluation by complex variable differentiation method," *Applied Mathematics and Computation*, vol. 316, pp. 256-281, 2018.

Shaolin Liao received his Ph.D. in Electrical Engineering from the University of Wisconsin, Madison, USA, in 2008. Dr. Liao has been a Full Professor of School of Electronics and Information Technology, Sun Yat-sen University since 2021. Before that, He was an R&D Staff at Argonne National Laboratory, and a Professor (Research) & Adjunct Teacher at the Department of Electrical and Computer Engineering of Illinois Institute of Technology, Chicago, IL, USA. Dr. Liao received his B.S. in Materials Science and Engineering, Tsinghua University, Beijing, China, in 2000. Dr. Liao is an Associate Editor of IEEE Access, a Academic Editor of PeerJ Computer Science, a Topic Editor of MDPI Electronics journal and MDPI Photonics journal. He has been a Senior Member of IEEE since 2015.

Lu Ou received the Ph.D. degree from Hunan University in software engineering in 2018. From 2015 to 2016, she was a visiting student at the Department of Computer Science, University of Texas at Arlington, USA. Currently, she is a postdoc in the College of Computer Science and Electronic Engineering at Hunan University, China. She is a member of IEEE. Her research focuses on data security, privacy and big data, as well as signal, image and video analysis.